Chapter 6

Inertial effects in ciliary flows - model problem

Abstract

In this chapter we investigate biomimetic fluid propulsion due to an array of periodically beating artificial cilia. A generic model system is defined in which the effect of inertial fluid forces and the spatial, temporal and orientational asymmetry of the ciliary motion can be individually controlled. We demonstrate that the so-far unexplored orientational asymmetry plays an important role in generating flow, that the flow increases sharply with Reynolds number and eventually becomes unidirectional. We introduce the concept of configurational symmetry that unifies the spatial, temporal and orientational symmetries. The breaking of configurational symmetry leads to fluid propulsion in microfluidic channels.

6.1 Introduction

One of the principal challenges in lab-on-a-chip applications is to propel the fluids in microchannels (Laser & Santiago, 2004). To propel fluids at these small length scales, nature utilizes cilia and flagella, attached to the surface of organisms to actuate the fluid locally so as to have a net fluid propulsion. A consequence of the small length scales is that viscous forces dominate over inertia forces, which dictates that the actuators have to move periodically in time but in a spatially asymmetric manner. This condition is satisfied in the case of cilia by the distinct effective and recovery stroke during each cycle of their motion (Brennen & Winet, 1977).

Many examples have appeared in recent literature of artificial cilia that mimic the natural ciliary motion through different physical actuation forces, imposed by electric fields, magnetic fields or through base excitation (Evans *et al.*, 2007; den Toonder *et al.*, 2008; Oh *et al.*, 2009; van Oosten *et al.*, 2009; Fahrni *et al.*, 2009; Kim & Netz, 2006; Gauger *et al.*, 2009; Khaderi *et al.*, 2009). In some cases the physical actuation forces get sufficiently large so that also the effect of inertia comes into play (den Toonder *et al.*, 2008; Baltussen *et al.*, 2009). As a result, the breaking of temporal asymmetry can also contribute to propulsion, in addition to the breaking of spatial asymmetry as required at low Reynolds numbers. In general, there are three fundamental mechanisms that are active in artificial cilia-driven fluid flow: (i) spatially asymmetric motion, (ii) temporally asymmetric motion and (iii) orientationally asymmetric motion. The first is the only mechanism that is effective at low Reynolds numbers. Nature effectively makes use of this at small length scales (e. g. cilia). In addition to spatial asymmetry, temporal asymmetry

Based on Khaderi, *et al. Breaking of symmetry in microfluidic propulsion driven by artificial cilia*, Physical Review E, 2010, **82**, 027302.

can enhance flow when inertia forces are no longer negligible (e. g. the locomotion of scallops is entirely based on spatially symmetric motion with temporal asymmetry). In human swimming both spatial and temporal asymmetry are employed. The third mechanism has not been carefully explored until now and is related to the asymmetry of the actuator motion relative to the channel direction. However, due to the intricate interplay of actuation forces (e. g. electric and magnetic), elastic forces, fluid inertia and drag forces, the individual contribution of the three fundamental mechanisms to the generated flow remains unknown. For instance, in the previous chapter the fluid flow was caused primarily due to the asymmetric motion. However, when the inertia forces became prominent, the temporal asymmetry caused a flow reversal and the resulting flow was due to a combination of inertia forces, temporal and spatial asymmetries.

To understand how the fluid flow depends individually on these mechanisms, we analyse a model system in which the relative contribution of the spatial, temporal and orientational asymmetry can be studied as a function of fluid inertia. We show that the inertia forces in the fluid can be usefully exploited to enhance the flow, when compared to the flow in the Stokes regime. Moreover, by utilizing the inertia forces the flow can be made unidirectional, even though the ciliary motion is cyclic. Interestingly, also natural cilia are able to generate a unidirectional flow, but utilize metachrony to achieve this (Satir & Sleigh, 1990). In the absence of any spatial and temporal asymmetry, the orientational symmetry can be broken which leads to flow rates that are comparable to typical spatially asymmetric rates in the Stokes regime. Finally, we unify the asymmetries studied in this analysis and introduce the general concept of configurational symmetry, the breaking of which causes flow.

6.2 Problem definition

The model system consists of an infinitely long array of synchronously beating cilia with an inter-ciliary spacing W, placed in a channel of height H. To perform the simulations, we choose a unit-cell of width $W = 2L$ and height $H = 2L$, whose top and bottom are no-slip boundaries and the left and right boundaries are periodic, see Fig. 6.1. We kinematically prescribe the motion of the cilium such that its tip moves in an elliptical orbit around $(x, y) = (0, 0)$, at an angular velocity of $\omega_e = 2\pi/T_e$ for the effective stroke and $\omega_r = 2\pi/T_r$ for the recovery stroke, resulting in a total cycle time $t_{\text{cycle}} = (T_e+T_r)/2$. Here, with $T_e/2$ and $T_r/2$ are the times taken to complete the effective and recovery stroke, respectively. The lengths of the principal elliptical axes are $2a$ and $2b$, oriented at an angle θ to the channel direction. The remaining portion of the cilium is kinematically prescribed to remain straight, with the lower end of the film fixed at $(-L\tan\theta, -L)$. The angle θ is zero when the principal elliptical axis $2a$ is parallel to the channel axis and is positive in the clockwise direction; the orientation shown in Fig. 6.1 corresponds to $\theta > 0$. The inertia in the fluid is independently controlled by changing the Reynolds number ($\text{Re} = \rho L^2/\mu t_{\text{cycle}}$) through the fluid density ρ, while the fluid viscosity μ is maintained constant. The temporal asymmetry is controlled by changing T_e/T_r, while the total cycle time $(T_e+T_r)/2$ is maintained constant. It is to be noted that when $a = 0$ or $b = 0$ no spatial asymmetry exists, when $T_e = T_r$ no temporal asymmetry exists and when $\theta = 0$ no orientational asymmetry exists.

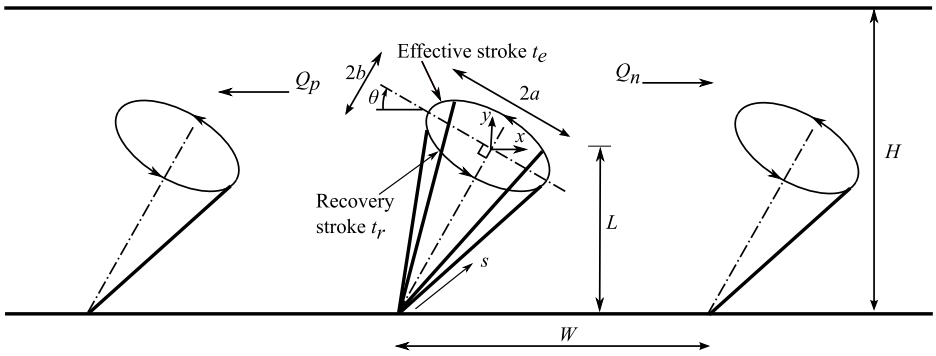

Figure 6.1: *Schematic picture of the model problem showing the parameters involved.*

6.3 Results

The defined problem is solved using the finite element method in which the fluid is assumed to be an incompressible Newtonian liquid. The fluid-structure interaction is performed using the fictitious domain method in which the fluid and the solid (cilia) velocities are coupled through Lagrange multipliers (Khaderi *et al.*, 2009; van Loon *et al.*, 2007). The instantaneous flux is obtained by integrating the horizontal velocity over the channel height, while the net amount of fluid propelled per cycle (termed 'area flow') is calculated by integrating the instantaneous flux over the cycle time. The fluid is initially at rest and it takes some time for the system to reach a steady state, especially at large Reynolds numbers. The outcome of the analysis is quantified in terms of three parameters after a steady state has been reached: area flow, the efficiency and the effectiveness of fluid transport. The latter are detailed in the following. The cilium pushes the fluid forward during the effective stroke, creating a 'positive area flow' Q_p in the direction of the effective stroke (i. e. to the left in Fig. 6.1) and pushes the fluid back during the recovery stroke creating a 'negative area flow' Q_n. Under suitable conditions, the positive flow is larger than the negative flow, generating a positive area flow per cycle $(Q_p - Q_n)$. The effectiveness, defined as $(Q_p - Q_n)/(Q_p + Q_n)$, indicates which part of the totally displaced fluid is effectively converted into a net flow. An effectiveness of unity represents a unidirectional flow. To investigate how efficiently the swept area (area of the ellipse) is converted to fluid flow, we define the efficiency as the area flow per unit area swept.

6.3.1 Effect of spatial and temporal asymmetry

We first study the dependence of the area flow on the area swept, Reynolds number and temporal asymmetry T_r/T_e for a fixed orientation $\theta = 0$ in Fig. 6.2. The swept area is changed by fixing b and changing a. Both the area flow and the swept area are normalised with the maximum area that can be swept by a cilium of length L $(\pi L^2/2)$. It can be seen that for all values of Reynolds number the area flow scales linearly with the swept area, Fig. 6.2(a) (as also observed in (Khaderi *et al.*, 2009) for the Stokes regime). It can be seen from the inset of Fig. 6.2(a) that for $\mathrm{Re} < 0.1$ (Stokes limit) the efficiency (i. e. the area flow/area swept) remains constant, while for $\mathrm{Re} > 0.1$ the efficiency increases sharply with an increase in Reynolds number. Moreover, at high

Reynolds numbers the flow generated increases when the effective stroke is faster than the recovery stroke ($T_e < T_r$), while it decreases when the opposite is true ($T_e > T_r$). Figure 6.2(b) shows the effectiveness as a function of area swept. The effectiveness is low when a large volume of fluid is shifted back and forth with only a modest net effect. This is the case in the Stokes regime. However, with increasing Reynolds number the effectiveness increases, reaching a purely unidirectional flow at Re ≈ 10 and for relatively fast effective strokes. As b is kept constant and a is increased, the velocity of the cilium is enhanced because the cycle time is fixed. Hence, as the swept area is increased, the instantaneous flux also increases due to the larger velocity during the effective as well as the recovery stroke. This results in the effectiveness of fluid actuation to be unchanged (Fig. 6.2(b)), but causes an increase in the net area flow due to the enhanced fluid velocity (Fig. 6.2(a)).

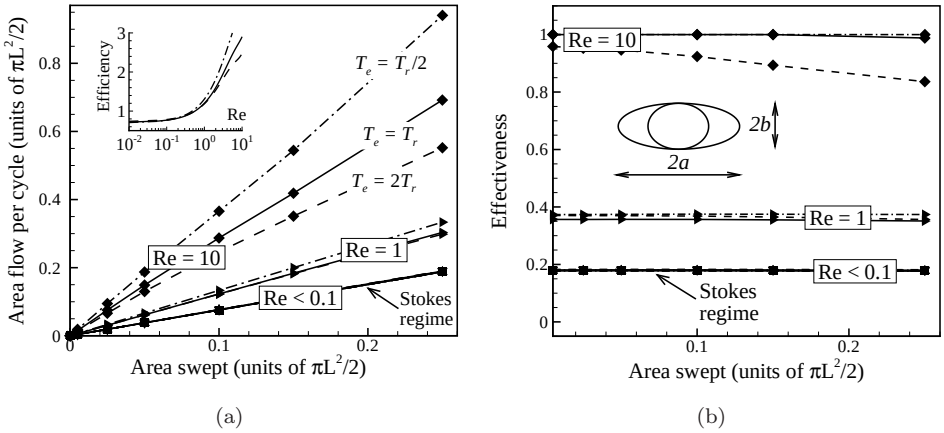

Figure 6.2: *(a) Area flow out of the channel as a function of the area swept ($\theta = 0°$) for different Reynolds numbers. Also plotted are the cases in which the velocity during the effective stroke is different from that of the recovery stroke. The inset shows the efficiency of fluid flow as a function of the Reynolds number. (b) Effectiveness of fluid flow ($(Q_p - Q_n)/(Q_p + Q_n)$) as a function of the area swept for different Reynolds numbers and T_e/T_r values.*

To analyse how the fluid is pumped through each cycle we plot the trajectory of fluid particles for two cycles in Fig. 6.3. We compare the results in the Stokes limit (low Re, Fig. 6.3(a)) with those at large Re (Re = 10, Fig. 6.3(b)). The fluid particles are represented by dots forming initially a straight line in instance 1. The instances 3 and 5 refer to the end of the first and the second cycle, respectively, and instances 2 and 4 refer to the end of the effective stroke of the first and second cycle. In the Stokes limit (i. e. low Re, see Fig. 6.3(a)), the dissipative viscous forces are larger than the inertia forces. As a consequence, the energy gained by the fluid due to the actuation of the cilium will be instantaneously dissipated, so that the momentum imparted by the cilium will be efficiently (instantaneously) transmitted to the surrounding fluid without delay. The fluid particles which initially form a straight line (instance 1) move due to the velocity imposed by the film during the effective stroke. The fluid particles stop and reverse their direction of motion once the film begins the recovery stroke (at instances 2 and 4) leading to back-flow during recovery (ending at instances 3 and 5). Due to the spatial asymmetry in the deformation of the film, we observe a net displacement of fluid

particles over each cycle. As the fluid particles move back and forth during the cycle, the flow exhibits a fluctuating behaviour, leading to a low effectiveness of fluid propulsion, see Fig. 6.2(b). The response of the system does not change when the effective and recovery stroke are performed at different rates.

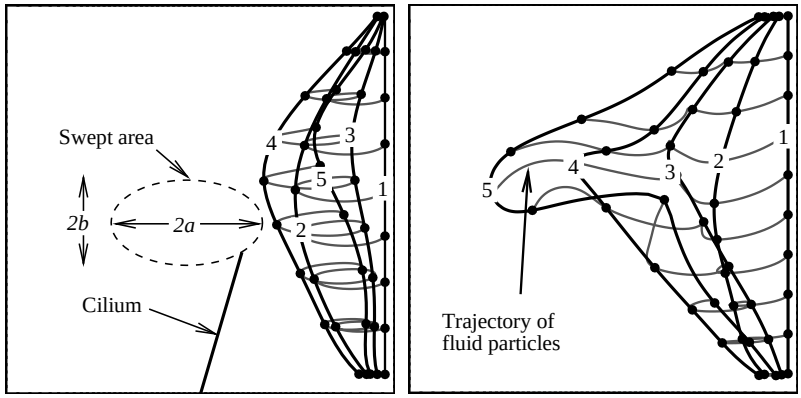

Figure 6.3: *Trajectory of particles over two cycles for $T_e = T_r$, $a = 0.3L$ and $b = 0.25L$. (a) Stokes regime (Re < 0.1); (b) Re = 10.*

When the Reynolds number is high (Fig. 6.3(b)), the dissipative forces are low compared to the inertia forces. Hence, the inertial momentum/energy gained by the fluid during the effective stroke is not dissipated instantaneously, but persists during recovery, which causes a flux in the direction of the effective stroke even during the recovery stroke, see instances 2-3 and 4-5. This effect becomes more prominent as the Reynolds number is increased, leading to a large net fluid flow (Fig. 6.2(a)), high efficiency (inset of Fig. 6.2(a)) and a higher effectiveness (Fig. 6.2(b)). The flow becomes fully unidirectional for $T_e = T_r$ when Re ≥ 10. Note that the particles close to the bottom boundary still fluctuate even at high Re. This is due to the fact that in this region the momentum is not transmitted through viscous forces, but due to the pressure gradient between adjacent cilia. This mode of momentum transfer is equally efficient at low as well as high Reynolds numbers, see Fig. 6.3.

6.3.2 Effect of orientational asymmetry

From the results presented so far, the effect of spatial and temporal asymmetry are independently studied, in the absence of orientational asymmetry ($\theta = 0$). To analyse the effect of orientational asymmetry we analyse the flow as a function of the orientation θ in the absence of spatial asymmetry ($a = 0.25L$ and $b = 0$) in Fig. 6.4. The temporal asymmetry is varied from $T_r = T_e$ (no asymmetry) to $T_r = 3T_e$ and the direction of ciliary motion θ from $-60°$ to $60°$ (see Fig. 6.1) for different Reynolds numbers. The area flow is normalised with $\pi L^2/2\cos^2\theta$. When the motion of the cilium exhibits no temporal asymmetry, we do not observe flow in the Stokes regime (Re < 0.1), for all orientations θ. Now, as we increase the Reynolds number (still $T_r = T_e$), a fluid flow is observed whose direction depends on the orientation θ, reaching a maximum at $\theta = \pm 45°$, see the broken lines in Fig. 6.4. The results are point-symmetric in $(0, 0)$ due to the absence

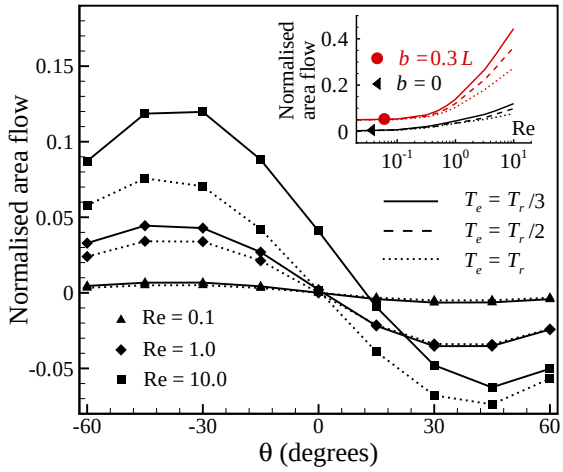

Figure 6.4: *Area flow normalised with $\pi L^2/2\cos^2\theta$ as a function of orientation θ for different Reynolds numbers and temporal asymmetries. The inset shows the normalised area flow as a function of Reynolds number (Re) for $\theta = -45°$ for different temporal and spatial asymmetries. In all the simulations a is taken to be equal to $0.25L$. Legend: The solid lines, dashed lines and broken lines refer to $T_e = T_r/3$, $T_e = T_r/2$ and $T_e = T_r$, respectively.*

of any spatial and temporal asymmetry. The flow generated is therefore entirely due to the breaking of orientational symmetry. When $\theta = -45°$ we obtain a maximal positive flow (i. e. flow in the direction of the effective stroke, see Fig. 6.1) and when the film moves in the direction $\theta = 45°$ we observe a negative flow. When we allow for temporal asymmetry (i. e. $T_e < T_r$), the flow is enhanced in the direction of the effective stroke (positive flow), the extent of which is larger for $\theta < 0$ compared to $\theta > 0$.

Consider the case when no temporal asymmetry exists ($T_r = T_e$), i. e. the dashed lines in Fig. 6.4, for $\theta = -45°$. During the effective stoke, the cilium imparts momentum to the fluid as it moves towards the bottom boundary and away from the moving fluid, allowing the fluid to pass without much obstruction in the direction of the effective stroke. When the cilium performs a recovery stroke, it again imparts momentum to the fluid, but now the cilium moves away from the bottom boundary thereby obstructing the flow during recovery. During the cycle, we thus have a larger flow during the effective stroke than during the recovery stroke, resulting in a net positive fluid flow in the effective direction. It is interesting to note that the observed net flow originates solely from the orientational asymmetry, causing an easy passage of fluid during the effective stroke while obstructing the flow during the recovery. Since there is no spatial or temporal asymmetry, the problem is perfectly symmetric with respect to $\theta = 0$, resulting in an equal-sized but opposite flow for $\theta = 45°$. When the fluid is pushed at a higher rate during the effective stroke, i. e. $T_e < T_r$ (the solid lines in Fig. 6.4), for $\theta < 0$ the motion of the film allows an easy passage of the high-momentum fluid during the effective stroke, while obstructing the low-momentum fluid during recovery. For $\theta > 0$, the film motion obstructs the high-energy fluid during the effective stroke and allows easy passage of low-energy fluid during recovery, resulting in a much smaller enhancement of positive flow than for $\theta < 0$. In the inset of Fig. 6.4 we analyse flow as a function of Reynolds number for $\theta = -45°$, in the presence ($b = 0.3L$) and absence ($b = 0$) of spatial asymmetry. It

can be observed that fluid propulsion can be generated when no temporal and spatial asymmetry exist, provided the fluid inertia is non-negligible (lowest curve). The flow can be increased by including temporal asymmetry (i. e. faster effective than recovery stroke). By adding spatial asymmetry, the effect of orientational and temporal asymmetry can be drastically enhanced, leading to a synergistic combination of all three asymmetries.

6.4 Configurational symmetry

The three independent symmetries studied in this chapter, i. e. spatial, temporal and orientational symmetry, can be generalized into the concept of configurational symmetry. We define a ciliary configuration at any time t by the position of material points $s(x, y)$ of the cilium and their instantaneous velocities $(\dot{x}, \dot{y})$. We define the system to be configurationally symmetric when every configuration (at time t) can find its mirror image after half a cycle (at time $t + t_{\text{cycle}}/2$), with the symmetry plane being perpendicular to the channel, see Fig. 6.5. A net flow will occur in the absence of configurational symmetry. This symmetry can be broken either by spatial, temporal or orientational asymmetry.

It is interesting to note that even a non-reciprocal motion can be configurationally symmetric. For instance, an actuator beating like a flagellum and aligned normal to the channel axis, will find its mirror image after half a cycle and therefore will not generate a net flow. Such an actuator needs to be non-perpendicular to the channel direction in order to break the orientational symmetry and to generate a flow, as has been shown in (Darnton *et al.*, 2004). Examples in the literature where the configurational symmetry is broken through spatial asymmetry leading to fluid flow can be found in (van Oosten *et al.*, 2009; Khaderi *et al.*, 2009; Gauger *et al.*, 2009; Kim & Netz, 2006), employing actuation forces that are generated by magnetic fields (Khaderi *et al.*, 2009; Gauger *et al.*, 2009), internal molecular motors (Kim & Netz, 2006) and light (van Oosten *et al.*, 2009). In the case of electrostatic artificial cilia (den Toonder *et al.*, 2008), the fluid flow was achieved by breaking both temporal and orientational symmetry. On the other hand, a nice example of configurationally symmetric cilia is given in (Oh *et al.*, 2009), where it is shown that a configurationally symmetric motion of cilia cannot generate a fluid flow in the direction of the channel. Thus, the definition of configurational symmetry can be a valuable fundamental concept in understanding existing (and designing new) physical actuation mechanisms for microfluidic propulsion. Moreover, it opens the opportunity of deriving analytical expressions that relate flow to quantitative measures of configurational asymmetry.

6.5 Summary

In this chapter we investigated the fundamental physical mechanisms that govern the microfluidic propulsion caused by artificial cilia. Many examples appeared in the recent literature of artificial cilia, but the understanding of the underlying mechanisms has been hampered by the strong competition between the actuation forces, elastic forces and fluid inertia and drag forces. By analysing a generic model system, we show that, besides the well known cilia-kind of spatially asymmetric motion, temporal and orientational asymmetries play a significant role in microfluidic propulsion.

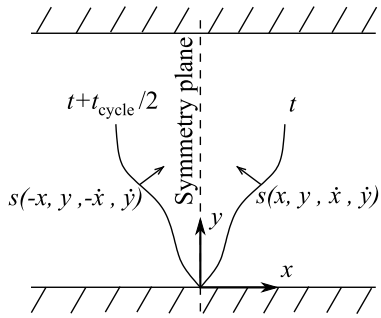

Figure 6.5: *Definition of configurational symmetry: every ciliary configuration (i. e. the current position of all material points $s(x, y)$ and their velocities $(\dot{x}, \dot{y})$) at time t can find its mirror image after half a cycle with the symmetry plane being perpendicular to the channel.*

The two key results of this chapter are: (i) Cilia can generate flow through orientational asymmetry alone, even in the absence of spatial and temporal asymmetry. This has not been fully explored before. (ii) All three fundamental symmetries can be generalized into the concept of configurational symmetry, the breaking of which causes fluid propulsion.